PCCP

PAPER

View Article Online
View Journal | View Issue

Cite this: *Phys. Chem. Chem. Phys.*, 2026, **28**, 8467

Self-assembly of structurally rigid diamondoid esters on a HOPG surface

Nataša Burić, †[a] Cosme González Ayani, †[b] Tomislav Vuletić, [b] Margareta Sohora, [a] Zoran Štefanić, [c] Ida Delač *[b] and Marina Šekutor *[a]

Received 2nd February 2026,
Accepted 9th March 2026

DOI: 10.1039/d6cp00381h

rsc.li/pccp

Characterizing assemblies of non-aromatic organic molecules on carrier surfaces is still an underexplored field of nanomaterial design. Here we present a study of on-surface self-assembly for diamondoid ester compounds on a highly oriented pyrolytic graphite (HOPG) surface. Using a combination of experimental and computational tools, we have developed an approach to characterize such non-aromatic molecules that also do not possess long alkyl chains in their structures. AFM imaging visualized the formed on-surface domains and by using the semi-empirical quantum mechanical GFN2-xTB method we could identify the most stable on-surface orientations of the individual molecules, a non-trivial task for non-aromatic compounds. Our synergistic analysis revealed that intermolecular London dispersion interactions enable molecular chains formation, which then arrange into distinct domains of observable structural periodicity. Our findings not only shed light onto self-assembly behavior of diamondoid esters but also provide a more general approach for characterizing currently less explored non-aromatics on carrier surfaces.

Introduction

The search for efficient and sustainable materials in everyday technologies is on-going. Of the many possibilities, carbon materials in particular show promise to revolutionize the way we approach nanotechnology applications. Of those, diamond recently attracted much attention due to its appealing properties like hardness and thermodynamic stability. However, some inherent drawbacks still limit its full potential for application in nanomaterial design, like limited scope of selective chemical functionalization and heterogeneous nanoparticle sizes formed upon mechanical grinding.[1] One possible solution to these challenges are diamondoids,[2] a class of organic hydrocarbons that are naturally occurring[3] and that possess a diamond-like structure built up from their cage carbons. These organic diamond analogues can be selectively functionalized through chemical means and demonstrate a so-called bottom-up principle to nanomaterial fabrication since their size can be precisely controlled. Consequently, the layers that emerge on various surfaces are uniform and their formation is governed by chemical properties modulated through functional group introduction to individual molecules rather than a statistical bulk matter functionalization. Functionalized diamondoids have already been applied as good monochromatic electron emitters,[4–8] and the heteroatom presence in the cages enables tuning of the emission spectrum.[6] It should be noted that larger diamondoid cages enhance emission properties,[9] making them more attractive for potential use. All these features of diamondoids led to them being considered as good candidates for bridging the gap between the flexibility of organics and the bulkiness of inorganic material.

It can be noticed that the applicability of diamondoids depends heavily on the ability to selectively functionalize their cages. Luckily, in recent decades significant progress has been made in targeted diamondoid C–H functionalization,[2] providing means to tackle the challenges of ordered layer formation of such derivatives and with a goal to apply them in functional electronic nanodevices.[4,10–14] However, there still remains much to be explored in order to achieve their controlled on-surface self-assembly and thus apply them as advanced organic materials. Namely, unlike aromatics, diamondoids are non-planar by nature and therefore less accessible to unambiguous on-surface structure identification by scanning tunneling microscopy (STM) and atomic force microscopy (AFM).[15–21] Inherent properties of their cage scaffolds like bulkiness and the mentioned non-planarity hinders somewhat the exact assignation of their on-surface orientation, which is information crucial for (mono)layer design. Nevertheless, quite recently some examples of STM and/or AFM studies of diamondoids and their derivatives

[a] *Department of Organic Chemistry and Biochemistry, Ruđer Bošković Institute, Bijenička 54, 10000 Zagreb, Croatia. E-mail: msekutor@irb.hr*
[b] *Centre for Advanced Laser Techniques, Institute of Physics, Bijenička cesta 46, 10000 Zagreb, Croatia. E-mail: idelac@ifs.hr*
[c] *Department of Physical Chemistry, Ruđer Bošković Institute, Bijenička 54, 10000 Zagreb, Croatia*
† Both contributors are considered first authors.

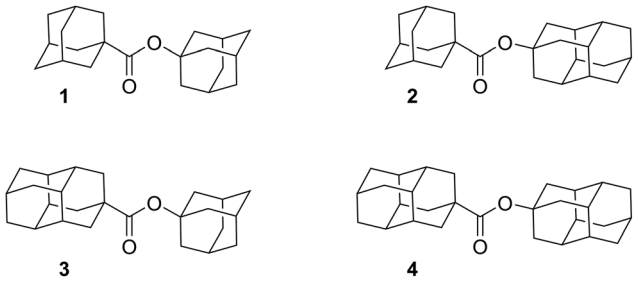

Fig. 1 Structures of the prepared diamondoid esters **1–4**.

on material surfaces have been described, ushering the topic into the research spotlight. Those include descriptions of self-assembly of adamantane,[22] tetramantanes,[23–26] diamondoid thiol[27,28] and diamondoid ether[29] molecules on metal or non-metal surfaces.

As mentioned, larger diamondoid cages appear to be more suitable for application in nanotechnology, however, we decided to approach the topic from a different route. Namely, we sought to explore diamondoid covalent assemblies, derivatives where two or more diamondoid cages were connected with heteroatoms or heteroatom groups. As a starting point, we characterized the orientation and behavior of diamondoid ethers on a highly oriented pyrolytic graphite (HOPG) surface,[29] finding that the assembly is heavily governed by London dispersion interactions. The ether oxygen was proposed to direct the initial molecular attraction after which the C–H bond rich bulky regions strengthen the non-covalent network and produce the final on-surface 2D lattice consisting of ordered diamondoid ether molecules. Encouraged by these results, we have embarked on a more complex and as of yet unexplored class of diamondoid covalent assemblies: diamondoid esters. The molecules themselves are scarcely investigated in general and only a few examples of their preparation exist in the literature. For instance, preparation of 1-adamantyl-1-adamantanecarboxylate was described, obtained either as a side product[30,31] or the target molecule.[32,33] Because of that we first had to develop a reliable and efficient method for preparation of various diamondoid esters, which we will describe in continuation. Additionally, characterization of self-assemblies consisting of non-planar organic molecules still remains a significant challenge despite some notable recent progress being made.[34–39] What is more, non-aromatic esters (*e.g.*, with pure alkyl chains as substituents) on surfaces have been seldom explored as well,[40–46] which was an additional motivation for us to study these molecules of interest (Fig. 1).

Results and discussion

As part of our investigation we prepared adamantane and diamantane substituted esters **1–4**. Esters **1**[47] and **2** were synthesized using the commercially available 1-adamantylcarboxylic acid and the respective alcohol,[48] while esters **3** and **4** had as a starting point 4-diamantylcarboxylic acid[49,50] prepared according to a previously developed procedure.[51] Our approach to the synthesis of diamondoid esters included the use of dried $MgSO_4$ and concentrated H_3PO_4 in 1,2-dichloroethane as a solvent to which the corresponding acid and alcohol were added. Reflux of the reaction mixture and subsequent work-up afforded target esters in good yields, while purification using column chromatography provided us with samples of high purity needed for deposition experiments on a HOPG surface.

In order to get more in-depth insights into on-surface self-assembly of diamondoid esters on HOPG, we used a combination of experimental (microscopy imaging) and theoretical (computations) tools, as we have already utilized previously for similar systems.[29] Such a combined approach was deemed necessary due to the complexity of aliphatic molecules characterization on surfaces, as detailed in the previous section. Thus, for diamondoid esters **1–4** we first acquired the corresponding AFM images in the AC mode, which are depicted in Fig. 2.

We initially imaged the HOPG surface after introducing several concentration ranges of the ester chloroform solutions. During that preliminary screening we also confirmed that chloroform itself does not leave any measurable traces on the surface, leading to the conclusion that any observed changes going forward are a consequence of molecular deposition. The collected data obtained under a 6–8 $\times$ 10^{-3} mol dm^{-3} concentration range confirms that all studied diamondoid esters form well-defined on-surface architectures on the HOPG surface. However, unlike previously studied diamondoid ethers that formed extensive uniform 2D lattices on HOPG,[29] esters **1–4** all form quite fragmented on-surface islands, as can be clearly observed from the recorded images (Fig. 2 and Fig. S5). These islands appear to possess the same molecular assembly patterns but are of different layer orientation, *e.g.*, their angles with respect to the scan direction differ substantially (Fig. S5). Observation of island domains that form without gaps between them indicates that these diamondoid ester molecules grow on the surface independently of the HOPG symmetry directions (indicated in the upper right corner of images in the first column of Fig. 2), pointing to their relatively weak coupling interaction to the substrate. Since in the observed islands the neighboring molecules arrange in a similar manner, intermolecular dispersion interactions acting between diamondoid cages seem to exert a significant effect on the layer formation process. Consequently, although the layer patterns themselves are uniform inside each island boundary, a mosaic-like pattern on a HOPG surface emerges in the end, *i.e.*, differently orientated homogenous islands produce an overall non-uniform surface coverage.

Even though self-assembled layers of esters **1–4** are fragmented, their individual rotational domains still possess row periodicity and distinct row width. Despite being at the limit of the used AFM instrument resolution, from the extracted profiles we managed to extract single row width values to be around 1.2–1.3 nm, which matches well with the expected range of molecule's length for esters **1–4**. For example, single row width for ester **3** was measured to be 1.30 $\pm$ 0.08 nm, while the corresponding dimension of the molecule in question (measured as the long-axis distance from the most protruding hydrogen atom of the first diamondoid cage to the analogous

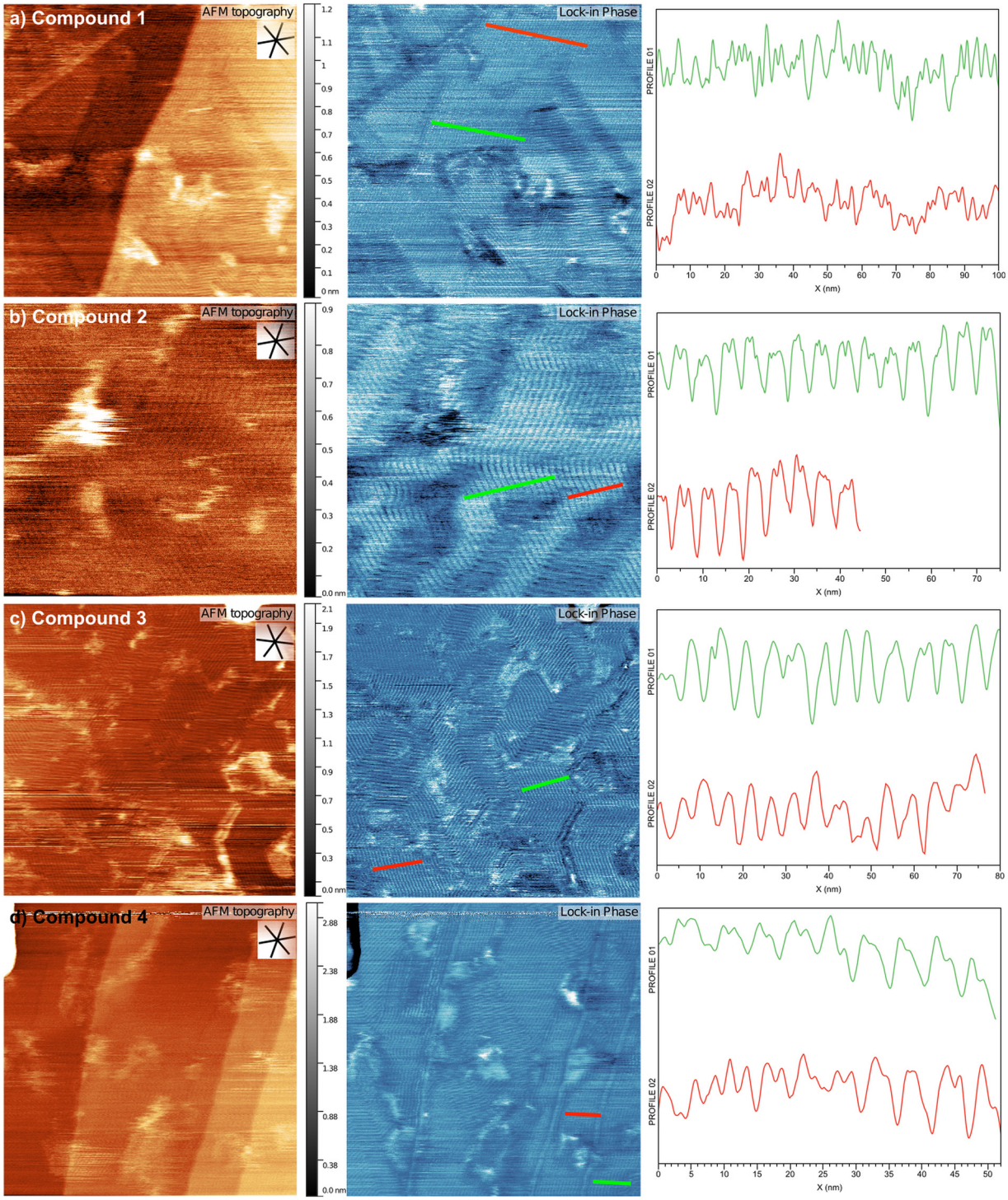

Fig. 2 On-surface characterization of (a) 1-adamantyl-1-adamantanecarboxylate (**1**), (b) 4-diamantyl-1-adamantanecarboxylate (**2**), (c) 1-adamantyl-4-diamantanecarboxylate (**3**), and (d) 4-diamantyl-4-diamantanecarboxylate (**4**) on HOPG. Each row corresponds to one diamondoid ester molecule (**1–4**, respectively), showing: (i) AFM topography images, (ii) the corresponding lock-in phase channel images revealing the self-assembled structures, and (iii) cross-section profiles extracted along the indicated lines. Image parameters: (a) 0.5 μm × 0.5 μm, (b) 0.25 μm × 0.25 μm, (c) 0.5 μm × 0.5 μm, (d) 0.5 μm × 0.5 μm.

hydrogen of the second one) is around 1.3 nm. This finding points towards an existence of molecular chains held together by non-covalent interactions between the cages, as we observed previously for diamondoid acids, albeit on metal surfaces,[52] and such chains further arrange in molecular islands of higher periodicity, like we saw here (Fig. 2 and Fig. S5).

Note that we also deposited diamondoid ester molecules on a mica surface and found that they assemble in a similar way

but with no discerning periodic patterns like on a HOPG surface (for example, see AFM images of molecule **4** on mica depicted in Fig. S6).

Let us next go in our discussion from a domain level to a molecular level. As rationalized, diamondoid ester molecules are adsorbed on the surface through non-covalent interactions, with dispersion attraction enabled by bulky diamondoid cages (good dispersion energy donors) having a dominant influence on chain formation. In other words, the observed supramolecular on-surface assembly is realized through a combination of the interaction of organic molecules with the HOPG surface and intermolecular interactions acting between the neighboring diamondoid moieties, as was the case for similar diamondoid covalent assemblies explored previously.[29] However, a key question of this study is what the role of the ester moiety in this organization process is. To shed more light on the strength of the directional effect from the ester functional group in this type of molecules with respect to the HOPG surface during the monolayer self-assembly, we turn our attention to discussing the obtained computational results.

We acquired the energy profiles of the studied esters **1–4** that were first deposited on HOPG and then optimized (with all surface atom coordinates frozen) using the semi-empirical quantum mechanical GFN2-*x*TB method.[53,54] This type of approach was already used for similar diamondoid systems[28,52] and we also applied it in our study of diamondoid ethers on surfaces.[29] One can construct and optimize several meaningful orientations of diamondoid ester molecules on a graphite surface and their feasibility can be determined from their computed interaction energies, which consists of the molecule-surface and molecule-molecule interaction contributions.

Studied esters can adopt orientations of interest where the carbonyl oxygen is facing towards the surface (orientation designated as **a**), away from the surface (orientation **b**) and in parallel to the surface (orientation **c**). Additionally, due to an inherent non-symmetric nature of the ester functional group, one can differentiate between two side orientations. The first is where both neighboring molecules are arranged to have the acid moieties interacting as well as having the remaining alcohol moieties in close contact, leading to a higher symmetry of the on-surface ensemble (designated as **_s**). The second orientation is where the respective acid moieties are neighboring the alcohol ones and is designated as **_a**. Fig. 3 depicts these possible on-surface orientations using 1-adamantyl-1-adamantanecarboxylate (**1**) as an example.

The obtained binding energies show that orientation **a** is the most favorable from all the computed on-surface geometries, not only for ester **1** but also for all other diamondoid esters studied here (Table S3). One can also observe an energetic preference for more symmetric molecule packing (arrangement **_s**). However, the differences in interaction energies values are not prohibitively large (typically inside a 5 kcal mol^{-1} window for various computed dimer orientations) and transient orientations existing on surfaces could be possible under these conditions. That being said, a marginal preference for a perpendicular orientation is in line with the reported literature examples dealing with long chain alkyl esters on surfaces.[42–44] Note that unlike long chain alkyl substituents, adamantane and diamantane cages are not limited with the surface features, as long chains often follow the surface grooves when adopting their most stable orientation. In contrast, diamondoids possess a bulkier constitution and are free to orient at a given surface without such mechanical constraints. Consequently, their on-surface orientation is a direct reflection of intermolecular as well as molecule–surface interaction strength. This is of importance since for relatively weak binding substrates like HOPG a balance between side and surface interactions[55] should be achieved if one wishes to design stable and relatively robust systems.

A computationally found general preference of diamondoid esters **1–4** on-surface orientation, with towards-the-surface directed carbonyls (**_a**) arranged in a symmetrical fashion (**_s**), can be matched with the experimental observation of molecularly uniform island domains consisting of chain

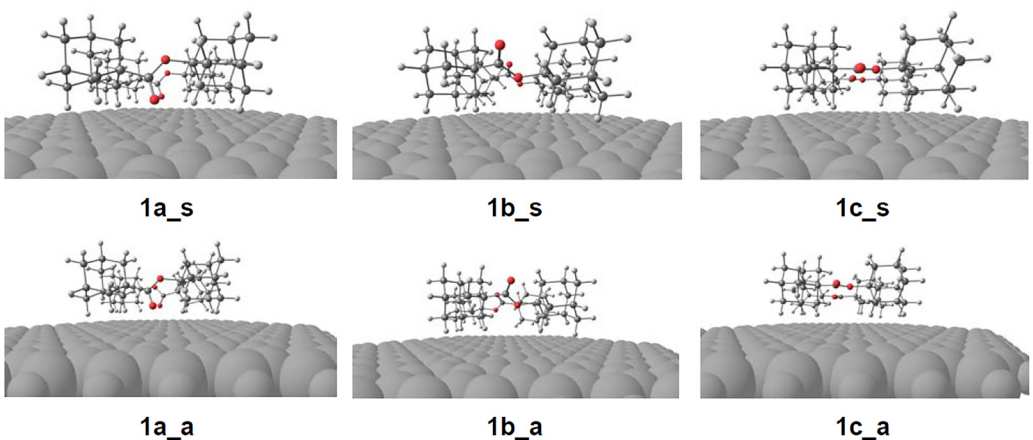

Fig. 3 Computed orientations of two ester **1** molecules interacting with the graphite surface. Carbonyl group directed, **a** – towards the surface, **b** – away from the surface, and **c** – parallel to the surface. Designation **_s** means the acid and alcohol moieties, respectively, are in contact with each other, while **_a** means the respective acid moieties are in contact with the alcohol moieties.

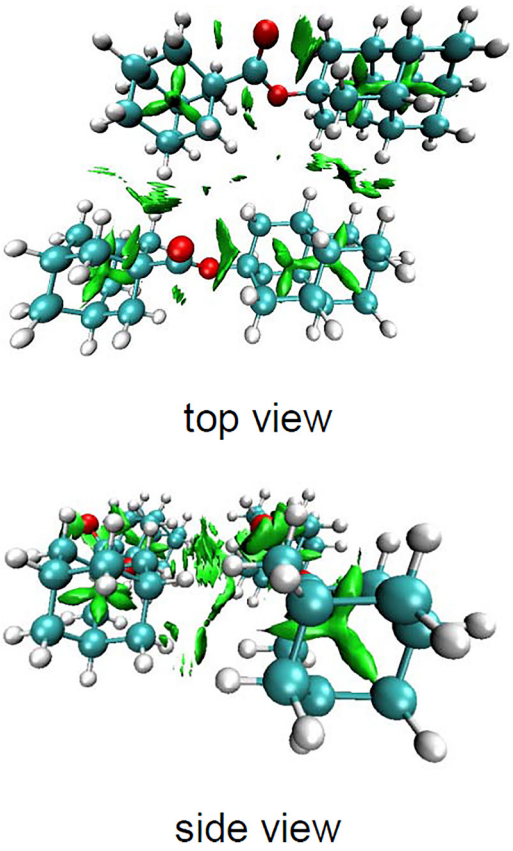

Fig. 4 NCI plots of self-assembled dimer structure of ester **2** present in orientation **a_s**. Non-covalent interactions are depicted in green.

patterns, suggesting that the ester adsorption indeed occurs preferentially for one distinct molecule orientation. Additionally, note that an interaction mode entailing contact of the ester carbonyl with the surface is already described in the literature.[40,44] As both our imaging and computational results suggest that dispersion-driven side interactions result in the formation of ordered on-surface domains, to confirm this rationale even further we generated NCI plots of computed self-assembled structures in orientation **a** (Fig. 4 and Fig. S7). By visually inspecting the close contact regions for *e.g.*, ester **2** (Fig. 4), one notices that the molecule-to-molecule side areas are rich in attracting zones (depicted in green), predominately acting between diamondoid cages. This is by no means surprising but rather additionally validates that dispersion side interactions are crucial for ordered domain assembly, *i.e.*, chain formation, of esters **1–4**.

Dispersion interactions are inherently non-directional but a targeted design of molecules that incorporate good dispersion energy donor subunits enables achieving a desired pattern emergence in on-surface behavior. As exemplified here, carbonyl oxygen atoms direct the molecular orientation with respect to the surface while diamondoid cages rich in C–H bonds enable molecule-to-molecule side interactions and tune the ordering of the resulting on-surface layer. Such non-covalent supramolecular binding therefore has a decisive role in providing locally arranged on-surface coverage, at least until the domain sizes do not grow too large and the islands start to fragment and change further chain growth direction.

We also computed molecular electron densities at the B3LYP-D3(BJ)/def2-TZVPP level of theory for assembly structures **a** that were initially optimized using the GFN2-xTB approach. By comparing the experimental images with computed electron density distribution of molecules (Fig. S8) a reasonable match is found. This compatibility between theory and experiment not only validates our method but also makes such computational analysis of diamondoid ester self-assemblies a useful tool for monolayer formation prediction, circumventing the need for synthesis of a library of compounds in the initial compound screening phase.

Furthermore, to gain more insight into the physico-chemical nature of the layer formation processes, we also performed experimental QCM-D (quartz crystal microbalance with dissipation) measurements. In brief, changes in the resonant frequency of the oscillating quartz crystal are proportional to mass of molecules deposited on the crystal. Thus, by detecting mass deposited, our intention was to characterize the ester layers complementarily to AFM imaging and to possibly track interaction kinetics. For that purpose we used an isopropanol solution of diamondoid esters **1–4** and the deposition was made to a gold sensor surface. For all instances we detected an apparently linear decrease in resonant frequency caused by material deposition on the sensor surface (Fig. 5). The deposition rates were rather low, which caused their linear, drifting appearance. However, when the solvent (without diamondoids) was introduced in a wash-step, the frequency shift would remain flat, indicating that the observed drift indeed was due to deposition of diamondoids and also that, when bound, the molecules are not removed by the solvent. Additionally, the resonant frequency levels measured in isopropanol before and after deposition were reduced for the amount of the drift that occurred during the deposition. In other words, the slow deposition rate still resulted in a measurable mass on the sensor. We note that the deposited mass translates into a coverage of less than 10^{14} molecules on a 1 cm^2 sensor surface, or stated differently, less than a molecule on a 1 × 1 nm^2 surface, while one could estimate about 4 molecules per nm^2 can be tightly packed, considering the sizes of these molecules. The linear appearance of the drift is due to the deposition rate not changing considerably on the time scales of our experiments – indicating that available surface for deposition did not decrease considerably, which correlates with submonolayer coverage. The possible explanation could lie in the solution flow nature of the experiment itself. Namely, it is known that intermolecular dispersion attraction can be significantly attenuated in organic solvents,[56–59] and since we have here shown that self-assembly of diamondoid esters on surfaces is strongly driven by dispersion interactions, it follows that the constant solvent flow around the molecules hinders their organization. However, when eventually deposited in an organized manner – they do not get washed away – as we observed.

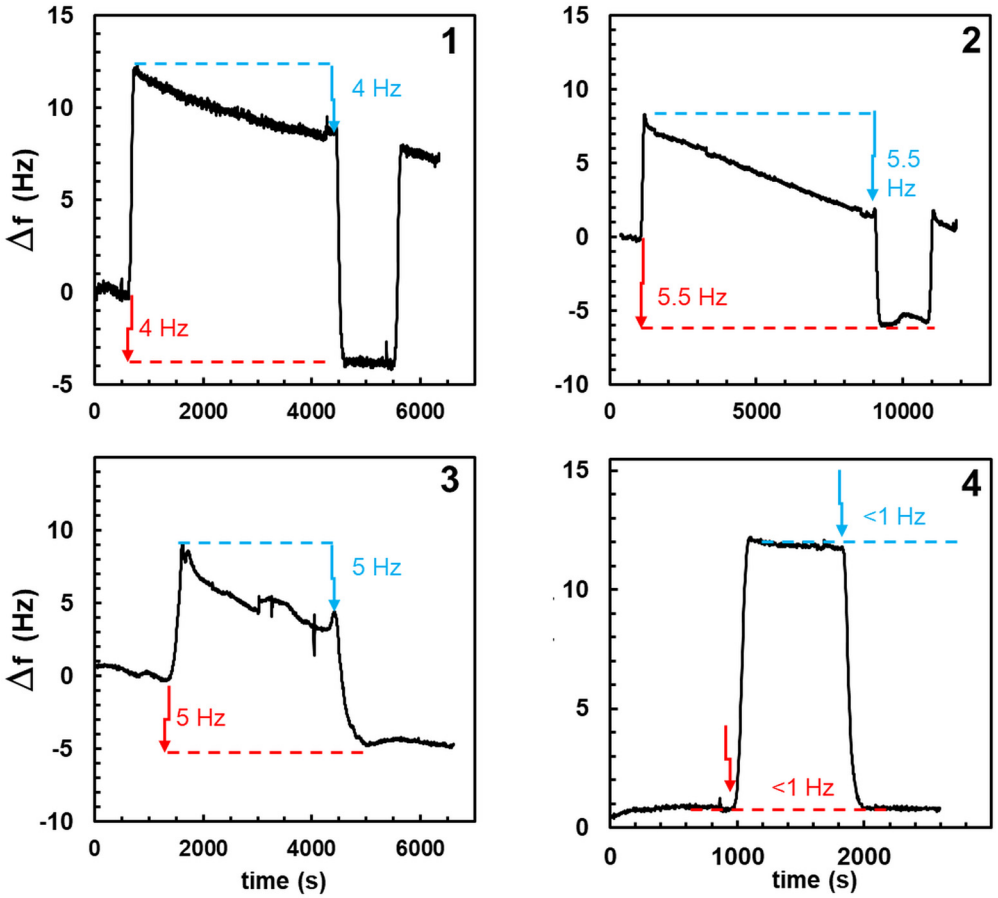

Fig. 5 QCM-D *in situ* monitoring of the deposition of diamondoid esters **1–4**. Frequency shift (f3 overtone-3rd harmonic). The vertical arrows show the moments for the addition of (red arrow) diamondoids in solvent/isopropanol and then diamondoid free solvent-isopropanol (blue arrow, washing-out step). Horizontal dashed lines denote the frequency shifts related to the diamondoid mass deposited.

This was not the case in the AFM experiments and the corresponding static setup used in that technique. Consequently, the obtained several Hz resonant frequency shifts, almost on the limits of the instrument, indirectly showcase that dispersion indeed governs the formation of diamondoid ester monolayer materials and that using non-covalent interactions for supramolecular architectures assembly often entails a careful selection of deposition methods. On another note, we also observed that the used isopropanol solvent does not wash out the ester molecules from the surface once they are deposited, which is a useful system property for possible practical application of such molecular layers.

On a concluding note, we also managed to obtain a single crystal of ester **2** in order to perform an X-ray analysis. The intention was to observe the close contacts between the ester molecules in all three dimensions rather than just a 2D structural network that emerges on a HOPG surface. As expected, the crystal lattice of ester **2** (space group *P*1, Table S1) is dominated by dispersion interactions, as confirmed by the values of the close contact distances in the crystalline system (Fig. 6). This observation once again highlights the importance of dispersion for bulk matter formation in general, especially when good

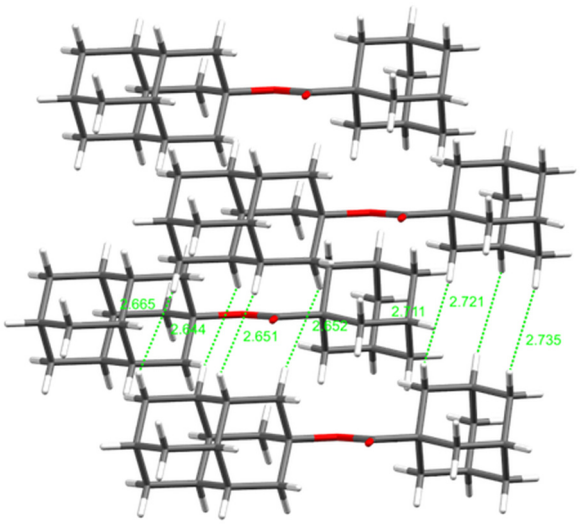

Fig. 6 Packing of compound **2** obtained from the X-ray crystal structures, space group *P*1. Selected close intermolecular contacts (dispersion interaction areas) are depicted as green dashed lines with the corresponding distances in Å. Grey (carbon), white (hydrogen), red (oxygen).

dispersion energy donor subunits are present in the structures of covalent assemblies like diamondoid esters and, as previously demonstrated, diamondoid ethers.[29]

Conclusions

We systematically characterized self-assemblies of diamondoid esters **1–4** using a combination of experimental and computational tools. AFM imaging enabled the detection of mosaic-like fused on-surface islands built up from molecular chain structures. Performed computations revealed the most stable molecular on-surface orientations, with ester carbonyls preferentially pointing towards the surface and with the molecules arranging in as symmetrical manner as possible. Our various observations from both the experiments and computations and a good data match between complementary approaches point towards dispersion as a governing factor for molecular chain formation, leading towards emergence of domains possessing noticeable structural periodicity. The here presented multidisciplinary approach for characterizing self-assemblies of diamondoid esters on carrier surfaces can be applied to a wider scope of less explored non-aromatic classes of molecules and is a useful tool for the bottom-up design of supramolecular architectures going beyond typical aromatic frameworks.

Experimental

Materials and methods

All ^{1}H and ^{13}C NMR spectra were recorded with Bruker AV-300 or AV-600 NMR spectrometers and the NMR spectra were referenced to the residual proton or carbon signal of the used deuterated solvent as an internal standard. IR spectra were recorded with a FT-IR ABB Bomem MB 102 spectrometer (range 400 to 4000 cm^{-1}). MALDI-TOF MS spectra were obtained in ''reflectron'' mode with an Applied Biosystems Voyager DE STR instrument (Foster City, CA). GC-MS analyses were performed on an Agilent 7890B/5977B GC/MSD instrument equipped with a HP-5ms column. Determination of melting points was performed by using an Original Kofler Mikroheiztisch apparatus (Reichert, Wien). All the solvents, 1-adamantanecarboxylic acid and adamantan-1-ol were obtained from commercial sources and used without further purification. 1-Adamantyl-1-adamantanecarboxylate (**1**) was prepared according to our previously published procedure.[47]

General procedure for diamondoid ester synthesis

A suspension of dried $MgSO_4$ (4 equivalents) and concentrated H_2SO_4 (1.1 equivalent) in 1,2-dichloroethane was stirred at rt for 20 min and then the corresponding diamondoid acid (1 equivalent) and the corresponding diamondoid alcohol (3 equivalents) were added. The reaction mixture was stirred under reflux for 16 h. After cooling of the reaction mixture, solid dry $MgSO_4$ (2 equivalents) and solid dry Na_2CO_3 (4 equivalents) were added and after stirring for 20 min at room temperature the salts were filtered off using a sinter funnel (porosity 4) and with a help of vacuum. The solvent from the filtrate was evaporated and the remaining crude product was purified by column chromatography on SiO_2, yielding the corresponding diamondoid ester.

4-Diamantyl-1-adamantanecarboxylate (2)

According to the general procedure, 1-adamantanecarboxylic acid (180 mg, 1 mmol), and diamantan-4-ol[48] (613 mg, 3 mmol) afforded after purification by column chromatography (*n*-hexane : dichloromethane = 1 : 1 as eluent) ester **2** (245 mg, 64%) as a white solid. M.p. 244–245 °C. ^{1}H NMR (300 MHz, $CDCl_3$) δ/ppm: 2.05 (d, J = 3.3 Hz, 6H), 1.93–2.01 (m, 6H), 1.83 (d, J = 2.9 Hz, 6H), 1.65–1.79 (m, 16H) with 1.73 (d, J = 2.6 Hz). ^{13}C NMR (75 MHz, $CDCl_3$) δ/ppm: 177.2 (C, 1C), 78.7 (C, 1C), 41.6 (CH_2, 3C), 41.17 (C, 1C), 39.7 (CH, 3C), 38.9 (CH_2, 3C), 37.2 (CH_2, 3C), 36.6 (CH_2, 3C), 36.5 (CH, 3C), 28.1 (CH, 3C), 25.6 (CH, 1C). IR (KBr), ν_{max}/cm^{-1}: 2903 (br), 1716 (s), 1452 (w), 1327 (w), 1273 (m), 1237 (s), 1107 (w), 1083 (s), 1048 (w), 1008 (w). MS (EI), m/z: 322.3. HRMS (MALDI): calcd for $[C_{25}H_{34}O_2 + H]^+$ 367.2637; found 367.2627.

1-Adamantyl-4-diamantanecarboxylate (3)

According to the general procedure, 4-diamantanecarboxylic acid[49,50] (375 mg, 1.6 mmol), and adamantan-1-ol (730 mg, 4.8 mmol) afforded after purification by column chromatography (*n*-hexane → *n*-hexane : diethyl ether = 4 : 1 as eluent) ester **3** (476 mg, 81%) as a white solid. M.p. 260–261 °C. ^{1}H NMR (600 MHz, $CDCl_3$) δ/ppm: 2.15 (br. s, 3H), 2.05–2.11 (m, 6H), 1.76–1.83 (m, 10H), 1.62–1.74 (m, 15H). ^{13}C NMR (150 MHz, $CDCl_3$) δ/ppm: 177.3 (C, 1C), 79.4 (C, 1C), 41.3 (CH_2, 3C), 39.8 (CH_2, 3C), 39.4 (C, 1C), 37.8 (CH_2, 3C), 37.4 (CH, 3C), 36.6 (CH, 3C), 36.3 (CH, 3C), 30.8 (CH, 3C), 25.7 (CH, 1C). IR (neat), ν_{max}/cm^{-1}: 2897 (br), 1710 (s), 1460 (w), 1354 (w), 1318 (w), 1277 (m), 1219 (s), 1092 (m), 1054 (m), 1024 (w), 971 (w), 883 (w). MS (EI), m/z: 322.3. HRMS (MALDI): calcd for $[C_{25}H_{34}O_2 + H]^+$ 367.2637; found 367.2640.

4-Diamantyl-4-diamantanecarboxylate (4)

According to the general procedure, 4-diamantanecarboxylic acid[49,50] (387 mg, 1.7 mmol), and diamantan-4-ol[48] (1050 mg, 5.1 mmol) afforded after purification by column chromatography (*n*-hexane → *n*-hexane : diethyl ether = 20 : 1 as eluent) ester **4** (193 mg, 28%) as a white solid. M.p. 300–301 °C. ^{1}H NMR (600 MHz, $CDCl_3$), δ/ppm: 2.04–2.07 (m, 6H), 1.95 (br. s, 3H), 1.77–1.83 (m, 11H), 1.67–1.77 (m, 18H). ^{13}C NMR (150 MHz, $CDCl_3$), δ/ppm: 177.4 (C, 1C), 78.8 (C, 1C), 41.6, 39.8, 39.7, 39.4 (C, 1C), 37.8, 37.4, 37.2, 36.6, 36.5, 25.7, 25.6. IR (neat), ν_{max}/cm^{-1}: 2878 (br), 1708 (s), 1463 (w), 1439 (w), 1378 (w), 1344 (w), 1317 (w), 1280 (m), 1219 (m), 1094 (m), 1082 (m), 1045 (w), 1029 (w), 1004 (w). MS (EI), m/z: 374.3. HRMS (MALDI): calcd for $[C_{29}H_{38}O_2 + H]^+$ 419.2950; found 419.2932.

Computations

The semi-empirical quantum mechanical GFN2-xTB method[53,54] was used for geometry optimization of ester molecules on the graphite surface consisting of 216 carbon atoms, with the graphite slab terminated with hydrogen atoms and

with all coordinates of the surface atoms frozen. Geometry optimization of individual ester molecules was done with the Orca 5 program package[60,61] using the B3LYP-D3(BJ)/def2-TZVPP level of theory[62–67] and the obtained minima were verified by frequency computations. Electron density distribution of the optimized on-surface ester assemblies was obtained using the same DFT level of theory. NCI plots were obtained using Multiwfn 3.6[68] and visualized by VMD software.[69]

AFM measurements

For the atomic force microscopy (AFM) measurements, molecules were dissolved in chloroform and the concentrations of the solutions were between 6 and 8×10^{-3} mol dm^{-3}, depending on the molecule. For each molecule, 3 μl droplet was carefully pipetted on a freshly cleaved substrate (HOPG, mica) and subsequently imaged immediately after solvent evaporated. Imaging was performed with a commercial AFM system (NanoWizard 4 Ultra Speed, JPK Instruments, Berlin, Germany) operating in AC mode. Measurements were conducted using TAP300Al-G probes from Budget Sensors (Sofia, Bulgaria), characterized by a curvature radius of 10 nm, a nominal spring constant of 40 N m^{-1}, and a resonant frequency of 300 kHz. The scanning rate was between 1 and 4 Hz, (**1**: 3.6 Hz, **2**: 3.6 Hz, **3**: 3.6 Hz, and **4**: 1.7 Hz for images in Fig. 2). AFM images were processed using Gwyddion software.[70]

QCM-D measurements

In situ adsorption. For the *in situ* monitoring of the adsorption of diamondoids to Au-surface, quartz crystal microbalance with dissipation monitoring (QCM-D) was employed utilizing a Q-Sense E1 instrument (Biolin Scientific AB, Gothenburg, Sweden) and as sensors the gold-coated AT-cut quartz crystal (QSX-301, Biolin Scientific AB, Gothenburg, Sweden) with a fundamental frequency of 4.96 MHz. For the analysis the 3rd harmonic frequency shift Δf was used. The Au sensor was cleaned every time before the measurement, following the manufacturer's recommendations: immersion into 2% SDS for 30 min followed with thorough rinsing with ultrapure water and drying with nitrogen gas. Dried sensors were treated by O_2 plasma for 10 minutes in Diener Zepto plasma oven (Ebhausen, Germany). The adsorption procedure was as follows. Isopropanol was flowed through the measurement cell until a stable baseline of the frequency (Δf) was established. Then, a sample solution (diamondoids dissolved in isopropanol) was introduced into the flow and the frequency drift was recorded. Finally, a wash step with only the solvent (isopropanol) was performed to establish another baseline (no frequency drift). Experiments were performed at 25 °C with a flow rate of 100 μL min^{-1}.

X-ray crystallography methods

Crystallization of ester **2** was performed by slow evaporation of dichloromethane/acetone solvent mixture. The crystal was mounted on a glass fiber and then fixed to the goniometer head of the X-ray diffractometer. The data on single crystal was collected on a Xcalibur Nova single crystal diffractometer equipped with Ruby CCD detector, using Cu Kα X-ray radiation with wavelength of λ = 1.5412 Å. The crystal was kept at room temperature during data collection. Using Olex2,[71] the structure were solved with the ShelXT[72] structure solution program using Intrinsic Phasing and refined with the ShelXL[72] refinement package using Least Squares minimization. Hydrogen atoms were introduced at calculated positions and treated using appropriate riding models. All non-hydrogen atoms were refined anisotropically. The crystal structure reported herein was deposited in the CSD and was allocated the CCDC deposition number 2518060.

Author contributions

The manuscript was written through contributions of all authors. All authors have given approval to the final version of the manuscript.

Conflicts of interest

The authors declare no competing financial interest.

Data availability

The data supporting the findings of this study have been made available in a repository FULIR data and can be accessed using the following link: https://urn.nsk.hr/urn:nbn:hr:241:180202.

Supplementary information (SI): contains details on synthesis, AFM measurements, X-ray crystallography methods and computations. See DOI: https://doi.org/10.1039/d6cp00381h.

CCDC 2518060 contains the supplementary crystallographic data for this paper.[73]

Acknowledgements

This work was supported by the Croatian Science Foundation under the project numbers HRZZ-UIP-2017-05-9653 and HRZZ-UIP-2020-02-8891. C. G. A. & I. D. also acknowledge financial support by the project HRZZ-MOBDOL-2023-08-2165; European Regional Development Fund (ERDF) project 'Materials for clean energy, advanced sensors and quantum technologies' (Grant No. PK.1.1.10.0002); Center of Excellence for Advanced Materials and Sensing Devices, ERDF Grant No. KK.01.1.1.01.0001. and Centre for Advanced Laser Techniques, ERDF Grant KK.01.1.1.05.0001. co-financed by the European Union through the ERDF—Competitiveness and Cohesion Operational Program and the Croatian Government. The computations were performed on the HPC Isabella and Supek based in SRCE–University of Zagreb, University Computing Centre for computational resources.

References

1 G. Reina, L. Zhao, A. Bianco and N. Komatsu, Chemical Functionalization of Nanodiamonds: Opportunities and

Challenges Ahead, *Angew. Chem., Int. Ed.*, 2019, **58**, 17918–17929.
2 A. A. Fokin, M. Šekutor and P. R. Schreiner, *The Chemistry of Diamondoids: Building Blocks for Ligands, Catalysts, Pharmaceuticals, and Materials*, Wiley, 2024.
3 J. E. Dahl, S. G. Liu and R. M. K. Carlson, Isolation and Structure of Higher Diamondoids, Nanometer-Sized Diamond Molecules, *Science*, 2003, **299**, 96–99.
4 W. A. Clay, Z. Liu, W. Yang, J. D. Fabbri, J. E. Dahl, R. M. K. Carlson, Y. Sun, P. R. Schreiner, A. A. Fokin, B. A. Tkachenko, N. A. Fokina, P. A. Pianetta, N. Melosh and Z.-X. Shen, Origin of the Monochromatic Photoemission Peak in Diamondoid Monolayers, *Nano Lett.*, 2009, **9**, 57–61.
5 T. M. Willey, J. R. I. Lee, J. D. Fabbri, D. Wang, M. H. Nielsen, J. C. Randel, P. R. Schreiner, A. A. Fokin, B. A. Tkachenko, N. A. Fokina, J. E. P. Dahl, R. M. K. Carlson, L. J. Terminello, N. A. Melosh and T. van Buuren, Determining orientational structure of diamondoid thiols attached to silver using near-edge X-ray absorption fine structure spectroscopy, *J. Electron Spectrosc. Relat. Phenom.*, 2009, **172**, 69–77.
6 M. Voros, T. Demjen, T. Szilvasi and A. Gali, Tuning the optical gap of nanometer-size diamond cages by sulfurization: a time-dependent density functional study, *Phys. Rev. Lett.*, 2012, **108**, 267401.
7 R. Richter, D. Wolter, T. Zimmermann, L. Landt, A. Knecht, C. Heidrich, A. Merli, O. Dopfer, P. Reiss, A. Ehresmann, J. Petersen, J. E. Dahl, R. M. K. Carlson, C. Bostedt, T. Moeller, R. Mitric and T. Rander, Size and shape dependent photoluminescence and excited state decay rates of diamondoids, *Phys. Chem. Chem. Phys.*, 2014, **16**, 3070–3076.
8 R. Richter, M. I. S. Roehr, T. Zimmermann, J. Petersen, C. Heidrich, R. Rahner, T. Moeller, J. E. Dahl, R. M. K. Carlson, R. Mitric, T. Rander and A. Merli, Laser-induced fluorescence of free diamondoid molecules, *Phys. Chem. Chem. Phys.*, 2015, **17**, 4739–4749.
9 K. T. Narasimha, C. Ge, J. D. Fabbri, W. Clay, B. A. Tkachenko, A. A. Fokin, P. R. Schreiner, J. E. Dahl, R. M. K. Carlson, Z. X. Shen and N. A. Melosh, Ultralow effective work function surfaces using diamondoid monolayers, *Nat. Nanotechnol.*, 2016, **11**, 267–272.
10 H. Schwertfeger, A. A. Fokin and P. R. Schreiner, Diamonds are a Chemist's Best Friend: Diamondoid Chemistry Beyond Adamantane, *Angew. Chem., Int. Ed.*, 2008, **47**, 1022–1036.
11 A. A. Fokin and P. R. Schreiner, in *Strategies and Tactics in Organic Synthesis*, ed. M. Harmata, Academic Press, 2012, vol. 8, p. 317–350.
12 M. A. Gunawan, J.-C. Hierso, D. Poinsot, A. A. Fokin, N. A. Fokina, B. A. Tkachenko and P. R. Schreiner, Diamondoids: functionalization and subsequent applications of perfectly defined molecular cage hydrocarbons, *New J. Chem.*, 2014, **38**, 28–41.
13 W. L. Yang, J. D. Fabbri, T. M. Willey, J. R. I. Lee, J. E. Dahl, R. M. K. Carlson, P. R. Schreiner, A. A. Fokin, B. A. Tkachenko, N. A. Fokina, W. Meevasana, N. Mannella, K. Tanaka, X. J. Zhou, T. van Buuren, M. A. Kelly, Z. Hussain, N. A. Melosh and Z.-X. Shen, Monochromatic Electron Photoemission from Diamondoid Monolayers, *Science*, 2007, **316**, 1460–1462.
14 S. Roth, D. Leuenberger, J. Osterwalder, J. E. Dahl, R. M. K. Carlson, B. A. Tkachenko, A. A. Fokin, P. R. Schreiner and M. Hengsberger, Negative-electron-affinity diamondoid monolayers as high-brilliance source for ultrashort electron pulses, *Chem. Phys. Lett.*, 2010, **495**, 102–108.
15 P. A. Held, H. Fuchs and A. Studer, Covalent-Bond Formation via On-Surface Chemistry, *Chem. – Eur. J.*, 2017, **23**, 5874–5892.
16 N. Pavliček and L. Gross, Generation, manipulation and characterization of molecules by atomic force microscopy, *Nat. Rev. Chem.*, 2017, **1**, 0005.
17 D. Cui, J. M. MacLeod and F. Rosei, Probing functional self-assembled molecular architectures with solution/solid scanning tunnelling microscopy, *Chem. Commun.*, 2018, **54**, 10527–10539.
18 Y. Ding, X. Wang, L. Xie, X. Yao and W. Xu, Two-dimensional self-assembled nanostructures of nucleobases and their related derivatives on Au(111), *Chem. Commun.*, 2018, **54**, 9259–9269.
19 D. P. Goronzy, M. Ebrahimi, F. Rosei, A. Arramel, Y. Fang, S. De Feyter, S. L. Tait, C. Wang, P. H. Beton, A. T. S. Wee, P. S. Weiss and D. F. Perepichka, Supramolecular Assemblies on Surfaces: Nanopatterning, Functionality, and Reactivity, *ACS Nano*, 2018, **12**, 7445–7481.
20 L. Gross, B. Schuler, N. Pavliček, S. Fatayer, Z. Majzik, N. Moll, D. Peña and G. Meyer, Atomic Force Microscopy for Molecular Structure Elucidation, *Angew. Chem., Int. Ed.*, 2018, **57**, 3888–3908.
21 L. Xing, Z. Peng, W. Li and K. Wu, On Controllability and Applicability of Surface Molecular Self-Assemblies, *Acc. Chem. Res.*, 2019, **52**, 1048–1058.
22 Y. Sakai, G. D. Nguyen, R. B. Capaz, S. Coh, I. V. Pechenezhskiy, X. Hong, F. Wang, M. F. Crommie, S. Saito, S. G. Louie and M. L. Cohen, Intermolecular interactions and substrate effects for an adamantane monolayer on a Au(111) surface, *Phys. Rev. B: Condens. Matter Mater. Phys.*, 2013, **88**, 235407.
23 Y. Wang, E. Kioupakis, X. Lu, D. Wegner, R. Yamachika, J. E. Dahl, R. M. K. Carlson, S. G. Louie and M. F. Crommie, Spatially resolved electronic and vibronic properties of single diamondoid molecules, *Nat. Mater.*, 2008, **7**, 38–42.
24 I. V. Pechenezhskiy, X. Hong, G. D. Nguyen, J. E. P. Dahl, R. M. K. Carlson, F. Wang and M. F. Crommie, Infrared Spectroscopy of Molecular Submonolayers on Surfaces by Infrared Scanning Tunneling Microscopy: Tetramantane on Au(111), *Phys. Rev. Lett.*, 2013, **111**, 126101.
25 D. Ebeling, M. Šekutor, M. Stiefermann, J. Tschakert, J. E. P. Dahl, R. M. K. Carlson, A. Schirmeisen and P. R. Schreiner, London Dispersion Directs On-Surface Self-Assembly of [121]Tetramantane Molecules, *ACS Nano*, 2017, **11**, 9459–9466.

26 D. Ebeling, M. Šekutor, M. Stiefermann, J. Tschakert, J. E. P. Dahl, R. M. K. Carlson, A. Schirmeisen and P. R. Schreiner, Assigning the absolute configuration of single aliphatic molecules by visual inspection, *Nat. Commun.*, 2018, **9**, 2420.
27 Y. Y. Lopatina, V. I. Vorobyova, A. A. Fokin, P. R. Schreiner, A. A. Marchenko and T. S. Zhuk, Structures and Dynamics in Thiolated Diamantane Derivative Monolayers, *J. Phys. Chem. C*, 2019, **123**, 27477–27482.
28 K. Feng, E. Solel, P. R. Schreiner, H. Fuchs and H.-Y. Gao, Diamantanethiols on Metal Surfaces: Spatial Configurations, Bond Dissociations, and Polymerization, *J. Phys. Chem. Lett.*, 2021, **12**, 3468–3475.
29 J. Alić, I. Biljan, Z. Štefanić and M. Šekutor, Preparation and characterization of non-aromatic ether self-assemblies on a HOPG surface, *Nanotechnology*, 2022, **33**, 355603.
30 L. F. Fieser, M. Z. Nazer, S. Archer, D. A. Berberian and R. G. Slighter, Naphthoquinone antimalarials. XXX. 2-Hydroxy-3-[ω-(1-adamentyl)alkyl]-1,4-naphthoquinones, *J. Med. Chem.*, 1967, **10**, 517.
31 Q. Y. Li, S. N. Gockel, G. A. Lutovsky, K. S. DeGlopper, N. J. Baldwin, M. W. Bundesmann, J. W. Tucker, S. W. Bagley and T. P. Yoon, Decarboxylative cross-nucleophile coupling via ligand-to-metal charge transfer photoexcitation of Cu(II) carboxylates, *Nat. Chem.*, 2022, **14**, 94–99.
32 L. Ochmann, M. L. Kessler and P. R. Schreiner, Alkylphosphinites as Synthons for Stabilized Carbocations, *Org. Lett.*, 2022, **24**, 1460–1464.
33 M. Tryniszewski and M. Barbasiewicz, Gram-Scale Preparation of Acyl Fluorides and Their Reactions with Hindered Nucleophiles, *Synthesis*, 2022, 1446–1460.
34 S. Kawai, T. Nishiuchi, T. Kodama, P. Spijker, R. Pawlak, T. Meier, J. Tracey, T. Kubo, E. Meyer and A. S. Foster, Direct quantitative measurement of the C═O···H–C bond by atomic force microscopy, *Sci. Adv.*, 2017, **3**, e1603258.
35 S. Kawai, O. Krejčí, T. Nishiuchi, K. Sahara, T. Kodama, R. Pawlak, E. Meyer, T. Kubo and A. S. Foster, Three-dimensional graphene nanoribbons as a framework for molecular assembly and local probe chemistry, *Sci. Adv.*, 2020, **6**, eaay8913.
36 J. Berger, K. Kośmider, O. Stetsovych, M. Vondráček, P. Hapala, E. J. Spadafora, M. Švec and P. Jelínek, Study of Ferrocene Dicarboxylic Acid on Substrates of Varying Chemical Activity, *J. Phys. Chem. C*, 2016, **120**, 21955–21961.
37 M. H. Chang, W. J. Jang, M. W. Lee, U. S. Jeon, S. Han and S.-J. Kahng, Networks of non-planar molecules with halogen bonds studied using scanning tunneling microscopy on Au (111), *Appl. Surf. Sci.*, 2018, **432**, 110–114.
38 M. Blanco Garcia, D. Perilli, C. Daldossi, A. Ugolotti, M. Giordano, D. S. Dolling, M. Wagstaffe, M. Kohantorabi, A. Stierle, C. Di Valentin and H. Noei, Unraveling the Role of the Multifunctional Groups in the Adsorption of L-Cysteine on Rutile TiO_2(110), *J. Am. Chem. Soc.*, 2025, **147**, 40158–40170.
39 S. Cai, J. S. Jestilä, P. Liljeroth and A. S. Foster, Direct Imaging of Chirality Transfer Induced by Glycosidic Bond Stereochemistry in Carbohydrate Self-Assemblies, *J. Am. Chem. Soc.*, 2025, **147**, 9341–9351.
40 E. Zahidi, M. Castonguay and P. McBreen, RAIRS and TPD Study of Methyl Formate, Ethyl Formate, and Methyl Acetate on Ni(111), *J. Am. Chem. Soc.*, 1994, **116**, 5847–5856.
41 F. Tao, Y. Cai and S. L. Bernasek, Scanning Tunneling Microscopy Studies of the Self-Assembly of Carboxylic Esters on Graphite: Linear Distortion and Multiple Adsorption Structures, *Langmuir*, 2005, **21**, 1269–1276.
42 C. Volcke, P. Simonis, F. Durant, P. A. Thiry, P. Lambin, C. Culot and C. Humbert, Use of Specific Functionalised Tips with STM: A New Identification Method of Ester Groups and Their Molecular Structure in Self-Assembled Overlayers, *Chem. – Eur. J.*, 2005, **11**, 4185–4190.
43 X. Miao, L. Xu, C. Liao, Z. Li, J. Zhou and W. Deng, Two-dimensional self-assembly of esters with different configurations at the liquid–solid interface, *Appl. Surf. Sci.*, 2011, **257**, 4559–4565.
44 M. Hibino and H. Tsuchiya, Bias voltage dependence of molecular orientation of dialkyl ketone and fatty acid alkyl ester at the liquid–graphite interface, *Appl. Surf. Sci.*, 2014, **317**, 803–810.
45 J. E. Fulker and W. A. Brown, Surface science studies of the coverage dependent adsorption of methyl acetate and methyl propanoate on graphite, *RSC Adv.*, 2024, **14**, 35373–35385.
46 J. E. Fulker, M. McCoustra and W. A. Brown, Evaluating Infrared Absorption Parameters for Low-Temperature Ices Using Reflection–Absorption Infrared Spectroscopy, *ACS Earth Space Chem.*, 2025, **9**, 746–756.
47 N. Burić, D. Loru, J. Alić, M. Šekutor, M. Schnell and P. Pinacho, Elucidating the structures of substituted adamantyl esters and ethers using rotational spectroscopy and computations, *ChemPhysChem*, 2025, **26**, e202500035.
48 N. A. Fokina, B. A. Tkachenko, A. Merz, M. Serafin, J. E. P. Dahl, R. M. K. Carlson, A. A. Fokin and P. R. Schreiner, Hydroxy Derivatives of Diamantane, Triamantane, and [121]Tetramantane: Selective Preparation of Bis-Apical Derivatives, *Eur. J. Org. Chem.*, 2007, 4738–4745.
49 T. M. Gund, M. Nomura, V. Z. Williams, P. v. R. Schleyer and C. Hoogzand, The functionalization of diamantane (congressane), *Tetrahedron Lett.*, 1970, **11**, 4875–4878.
50 T. M. Gund, M. Nomura and P. v. R. Schleyer, Diamantane. II. Preparation of derivatives of diamantane, *J. Org. Chem.*, 1974, **39**, 2987–2994.
51 N. A. Fokina, B. A. Tkachenko, J. E. P. Dahl, R. M. K. Carlson, A. A. Fokin and P. R. Schreiner, Synthesis of Diamondoid Carboxylic Acids, *Synthesis*, 2012, 259–264.
52 H.-Y. Gao, M. Šekutor, L. Liu, A. Timmer, H. Schreyer, H. Mönig, S. Amirjalayer, N. A. Fokina, A. Studer, P. R. Schreiner and H. Fuchs, Diamantane Suspended Single Copper Atoms, *J. Am. Chem. Soc.*, 2019, **141**, 315–322.
53 S. Grimme, C. Bannwarth and P. Shushkov, A Robust and Accurate Tight-Binding Quantum Chemical Method for Structures, Vibrational Frequencies, and Noncovalent Interactions of Large Molecular Systems Parametrized for All

spd-Block Elements (Z = 1-86), *J. Chem. Theory Comput.*, 2017, **13**, 1989–2009.
54 C. Bannwarth, S. Ehlert and S. Grimme, GFN2-xTB-An Accurate and Broadly Parametrized Self-Consistent Tight-Binding Quantum Chemical Method with Multipole Electrostatics and Density-Dependent Dispersion Contributions, *J. Chem. Theory Comput.*, 2019, **15**, 1652–1671.
55 A. Rochefort and J. D. Wuest, Interaction of Substituted Aromatic Compounds with Graphene, *Langmuir*, 2009, **25**, 210–215.
56 R. Pollice, F. Fleckenstein, I. Shenderovich and P. Chen, Compensation of London Dispersion in the Gas Phase and in Aprotic Solvents, *Angew. Chem., Int. Ed.*, 2019, **58**, 14281–14288.
57 R. Pollice, M. Bot, I. J. Kobylianskii, I. Shenderovich and P. Chen, Attenuation of London Dispersion in Dichloromethane Solutions, *J. Am. Chem. Soc.*, 2017, **139**, 13126–13140.
58 C. Adam, L. Yang and S. L. Cockroft, Partitioning Solvophobic and Dispersion Forces in Alkyl and Perfluoroalkyl Cohesion, *Angew. Chem., Int. Ed.*, 2015, **54**, 1164–1167.
59 L. Yang, C. Adam, G. S. Nichol and S. L. Cockroft, How much do van der Waals dispersion forces contribute to molecular recognition in solution?, *Nat. Chem.*, 2013, **5**, 1006–1010.
60 F. Neese, The ORCA program system, *Wiley Interdiscip. Rev.: Comput. Mol. Sci.*, 2012, **2**, 73–78.
61 F. Neese, Software update: the ORCA program system, version 4.0, *Wiley Interdiscip. Rev.: Comput. Mol. Sci.*, 2018, **8**, e1327.
62 A. D. Becke, Density-functional thermochemistry. III. The role of exact exchange, *J. Chem. Phys.*, 1993, **98**, 5648–5652.
63 C. Lee, W. Yang and R. G. Parr, Development of the Colle-Salvetti correlation-energy formula into a functional of the electron density, *Phys. Rev. B: Condens. Matter Mater. Phys.*, 1988, **37**, 785–789.
64 S. Grimme, J. Antony, S. Ehrlich and H. Krieg, A consistent and accurate ab initio parametrization of density functional dispersion correction (DFT-D) for the 94 elements H-Pu, *J. Chem. Phys.*, 2010, **132**, 154104.
65 S. Grimme, S. Ehrlich and L. Goerigk, Effect of the damping function in dispersion corrected density functional theory, *J. Comput. Chem.*, 2011, **32**, 1456–1465.
66 F. Weigend and R. Ahlrichs, Balanced basis sets of split valence, triple zeta valence and quadruple zeta valence quality for H to Rn: Design and assessment of accuracy, *Phys. Chem. Chem. Phys.*, 2005, **7**, 3297–3305.
67 F. Weigend, Accurate Coulomb-fitting basis sets for H to Rn, *Phys. Chem. Chem. Phys.*, 2006, **8**, 1057–1065.
68 T. Lu and F. Chen, Multiwfn: A multifunctional wavefunction analyzer, *J. Comput. Chem.*, 2012, **33**, 580–592.
69 W. Humphrey, A. Dalke and K. Schulten, VMD: Visual molecular dynamics, *J. Mol. Graphics*, 1996, **14**, 33–38.
70 D. Nečas and P. Klapetek, Gwyddion: an open-source software for SPM data analysis, *Open Phys.*, 2012, **10**, 181–188.
71 O. V. Dolomanov, L. J. Bourhis, R. J. Gildea, J. A. K. Howard and H. Puschmann, OLEX2: a complete structure solution, refinement and analysis program, *J. Appl. Crystallogr.*, 2009, **42**, 339–341.
72 G. Sheldrick, SHELXT - Integrated space-group and crystal-structure determination, *Acta Crystallogr., Sect. A*, 2015, **71**, 3–8.
73 CCDC 2518060: Experimental Crystal Structure Determination, 2026, DOI: 10.5517/ccdc.csd.cc2qj7r8.